applied sciences

MDPI

Article

Analysis of Initial Cracking of an Interface between a Bundled Lipped Channel–Concrete Composite Wall and an Infill Wall

Pengyun Cheng, Lifeng Zhang *, Gaohang Lin, Kuangliang Qian, Xiaoqian Qian and Shaoqin Ruan *

College of Civil Engineering and Architecture, Zhejiang University, Hangzhou 310058, China; pengyuncheng@zju.edu.cn (P.C.); lingaohang@zju.edu.cn (G.L.); qklcivil@zju.edu.cn (K.Q.); qianxq1@zju.edu.cn (X.Q.)
* Correspondence: zhanglifeng@zju.edu.cn (L.Z.); sruan001@zju.edu.cn (S.R.)

Abstract: The bundled lipped channel–concrete (BLC-C) composite wall structure is a new structure with several advantages such as a high bearing capacity and good seismic performance. However, interface cracks between a BLC-C composite wall and the infill wall (non-structural wall) are a severe problem and need to be urgently resolved. Interface cracks affect not only the esthetics, but also the normal use of a building. The presence of interface cracks changes the perceptions of the owners of a structure, forcing them to question its safety and even take legal action against its developer. Therefore, in this study we aimed to investigate the initial cracking of the interface between a BLC-C composite wall and an infill wall. Unidirectional horizontal loading tests were conducted on two infill wall specimens constrained by BLC-C composite walls on both sides. The finite element analysis software ANSYS was used to simulate the loading process of the tests. The test results were compared to verify the accuracy of the finite element model. A finite element analysis was conducted to determine the effect of the horizontal displacement of the specimens when the interface initially cracked under different parameters such as the widths of the BLC-C composite wall, infill wall, and opening as well as the strength grade of the bricks and maximum normal contact stress. The results showed that a decrease in the width of the BLC-C composite wall or a rise in the width of the infill wall delayed the appearance of interface cracks. A large opening also delayed the occurrence of interface cracks. An enhancement in the strength grade of the bricks led to an earlier appearance of interface cracks. Interface cracks occurred later with an increase in the maximum normal contact stress between the BLC-C composite wall and the infill wall.

Keywords: bundled lipped channel–concrete composite wall; infill wall; finite element analysis; interface; initial cracking

check for updates

Citation: Cheng, P.; Zhang, L.; Lin, G.; Qian, K.; Qian, X.; Ruan, S. Analysis of Initial Cracking of an Interface between a Bundled Lipped Channel–Concrete Composite Wall and an Infill Wall. *Appl. Sci.* **2022**, *12*, 7110. https://doi.org/10.3390/app12147110

Academic Editor: Jong Wan Hu

Received: 26 June 2022
Accepted: 13 July 2022
Published: 14 July 2022

Publisher's Note: MDPI stays neutral with regard to jurisdictional claims in published maps and institutional affiliations.

Copyright: © 2022 by the authors. Licensee MDPI, Basel, Switzerland. This article is an open access article distributed under the terms and conditions of the Creative Commons Attribution (CC BY) license (https://creativecommons.org/licenses/by/4.0/).

1. Introduction

In recent years, with the rapid advancement of construction industrialization and the development of prefabricated buildings, a new type of bundled lipped channel–concrete (BLC-C) composite wall structure has been proposed [1]. A BLC-C composite wall is formed by welding several U-shaped or rectangular steel tubes and pouring self-compacting concrete into the steel tube cavity. A BLC-C composite wall structure can fully utilize the material advantages of steel and concrete, reduce the cross-section of components, and increase space utilization. A BLC-C composite wall structure also has the advantages of a fast construction speed, high degree of assembly, low economic cost [2], high bearing capacity, and superior seismic performance; it is expected to be widely used in high-rise and super-high-rise buildings [3].

There have been a few studies conducted by researchers worldwide on BLC-C composite wall structures. Zhang et al. [4] conducted a hysteretic test on a T-shaped BLC-C composite wall and studied the influence of the cross-section, thickness of the steel plate, axial load ratio, and presence of shear studs on the seismic performance of a BLC-C composite wall. Li et al. [5] tested two types of wall–beam joints on a BLC-C composite wall structure, revealing that the two wall–beam joints exhibited a good bearing capacity and ductility. Chen et al. [6] analyzed the parameters of a BLC-C composite wall based on an accurate finite element modeling method verified by experiments and studied the influence of each parameter on the mechanical properties of a BLC-C composite wall. Guo et al. [7] further studied the failure process, failure mechanism, and seismic performance of a BLC-C composite wall by considering the restraint capacity from the steel to the core concrete. Sun et al. [8] conducted an axial compression test on a T-shaped BLC-C composite wall and performed finite element calculations and analyses. Based on the finite element calculation results, a formula for calculating the axial bearing capacity of a BLC-C composite wall was proposed.

The problem of cracks at the junction of the main structure and the infill wall often occurs in reinforced concrete frame structures, reinforced concrete frame–shear wall structures, reinforced concrete shear wall structures, and steel structures. In a BLC-C composite wall structure, interface cracks between the BLC-C composite wall and the infill wall are also a problem and have been troubling owners and developers. Due to the significant difference in stiffness between a BLC-C composite wall and an infill wall, they cannot synergistically deform. In addition, the cohesive force of a BLC-C composite wall to an infill wall is weak, so interface cracks are likely to occur. An interface crack directly affects the esthetics of a building. The adverse effects on the senses of the owner cannot be ignored either. Moreover, a house is the private asset of an owner and the existence of interface cracks can easily cause economic disputes. Interface cracks cause owners to question the safety of the structure and even sue the developer, even though they do not have much of an effect on the bearing capacity of the structure. Therefore, it is necessary to further study the initial cracking of an interface. However, no related research is available on the interface cracks between a BLC-C composite wall and an infill wall although a large number of studies have been conducted on frames with infill walls. A method for calculating the lateral stiffness of masonry-infilled reinforced concrete frames with a central opening has been proposed [9]. The influence of an infill wall on the strength, stiffness, ductility, and dynamic characteristics of a reinforced concrete frame was experimentally investigated [10]. The interaction between an infill wall and a boundary frame was studied [11]. Asteris et al. [12] studied an infilled reinforced concrete frame under a lateral load and also investigated a numerical model of the out-of-plane response of a frame with infill walls [13]. Buonopane and White [14] conducted a pseudo-dynamic test on a two-story infilled reinforced concrete frame and explored the relationship between the crack type and hysteresis energy. The test results showed that an upper story with openings mainly produced diagonal cracks whereas a lower story without openings primarily produced bed joint shear cracks. Koutromanos et al. [15] applied the smeared crack continuum model and the cohesive crack interface model to establish a finite element model of reinforced concrete frames with masonry walls. The established model accurately simulated the load–displacement response, crack mode, and failure mechanism in a cyclic lateral loading test.

As a new type of structure, the connection mode between a BLC-C composite wall and an infill wall is worthy of further study. At present, there are two main types of structural connections between a BLC-C composite wall and an infill wall that have been applied in practical engineering. As depicted in Figure 1, two HPB300 steel bars with a diameter of 6 mm are arranged every 500 mm along the wall height and the ends of the steel bars are welded to the BLC-C composite wall. The joint between the BLC-C composite wall and the infill wall is filled with 20 mm-thick cement mortar and sealed with a sealant. On both sides of the wall, welded wire fabrics coated with zinc are arranged and they are leveled and plastered with gypsum plaster. Figure 2 is different from Figure 1 in that the cement mortar is replaced with anti-crack mortar. The dry mix of anti-crack mortar comprises cement, fly ash, sand, rubber powder, fibers, cellulose ether, and an admixture.

In this study, we aimed to investigate cracks in the interface between a BLC-C composite wall and an infill wall. An experiment was conducted on two infill wall specimens constrained by BLC-C composite walls on both sides under unidirectional horizontal loads.

Based on the experimental phenomena and load–displacement curves, a finite element modeling analysis was conducted to simulate the horizontal loading process. To investigate the initial cracking of the interface, a finite element analysis was performed to study the influence of each factor on the horizontal displacement when the interface initially cracked.

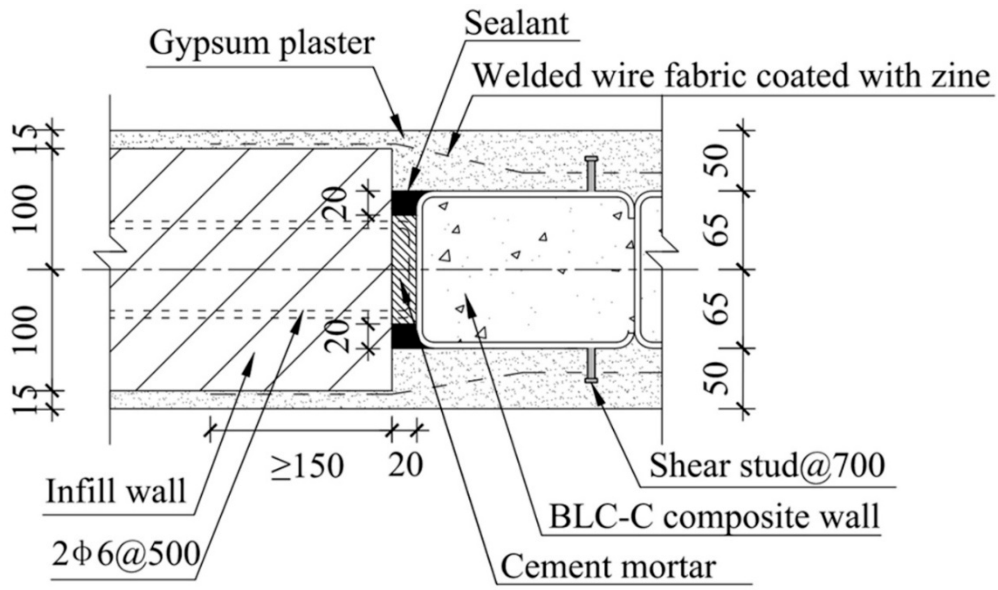

Figure 1. Connection structure of the interface (using cement mortar; units in mm).

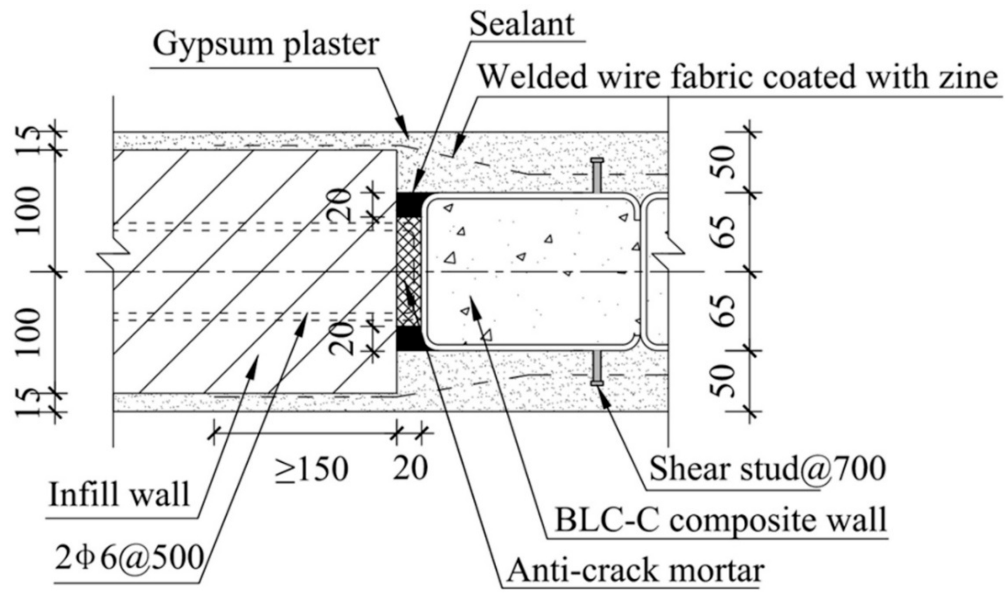

Figure 2. Connection structure of the interface (using anti-crack mortar; units in mm).

2. Experiments

2.1. Experimental Design

According to Chinese standard GB 50011 "Code for seismic design of buildings" [16], the main structure of the building was not damaged and non-structural components (including the infill wall) were not excessively damaged within the elastic story drift limit. Furthermore, the interface between the BLC-C composite wall and the infill wall initially cracked within the elastic story drift limit. Therefore, the experiment conducted in this study focused on the mechanical behavior within the elastic story drift limit.

According to actual engineering design drawings, the specimens were designed to simulate the walls of a high-rise BLC-C composite wall structure. Two specimens, W1 and

W2, were produced and comprised an infill wall and a BLC-C composite wall on both sides. The materials of all BLC-C composite walls were Q355 (nominal yield strength is 355 MPa) steel and C45 concrete (nominal cubic compressive strength is 40 MPa). The infill wall was composed of MU10 burned shale perforated bricks (nominal compressive strength is 10 MPa) and M5 cement mortar (nominal cubic compressive strength is 5 MPa). The specific dimensions of the two specimens are shown in Figure 3. The height of the specimens was 3350 mm. The widths of the BLC-C composite walls of the two specimens were 1730 and 2390 mm, respectively, and the thickness was 130 mm. The BLC-C composite walls were composed of steel tubes of different sizes such as 200 mm × 130 mm × 4 mm, 130 mm × 130 mm × 8 mm, 130 mm × 130 mm × 4 mm, and 140 mm × 130 mm × 5 mm. To distinguish them more clearly, the one near the loading end was referred to as the rear BLC-C composite wall and the other was referred to as the front BLC-C composite wall. The widths of the infill walls of the two specimens were 2440 and 3680 mm, respectively, and the thickness was 200 mm. The structural connection between the BLC-C composite wall and the infill wall shown in Figure 2 was adopted for the test. The thicknesses of the gypsum plaster on both sides of the BLC-C composite wall and the infill wall were 50 mm and 15 mm, respectively.

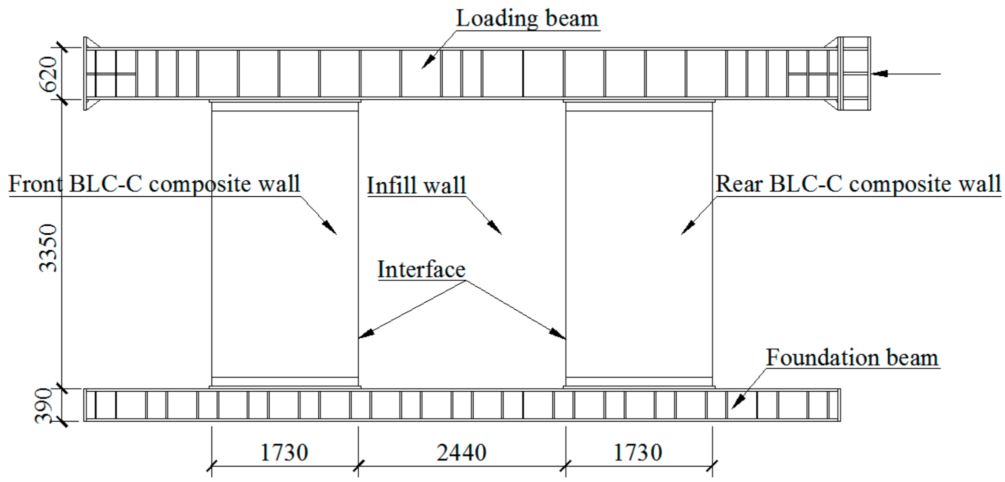

(**a**)

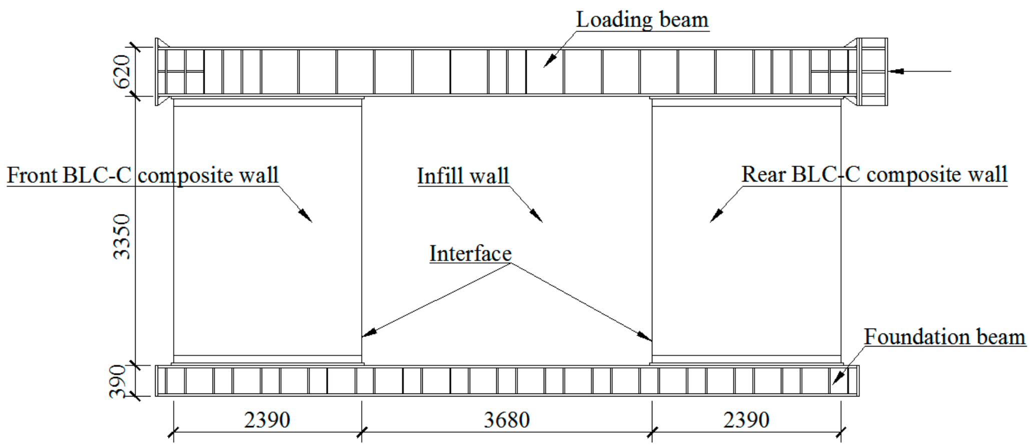

(**b**)

Figure 3. *Cont.*

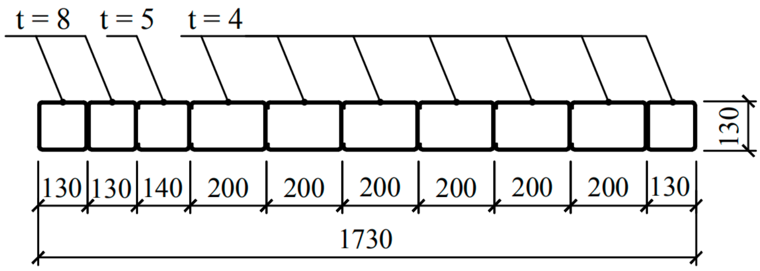

(c)

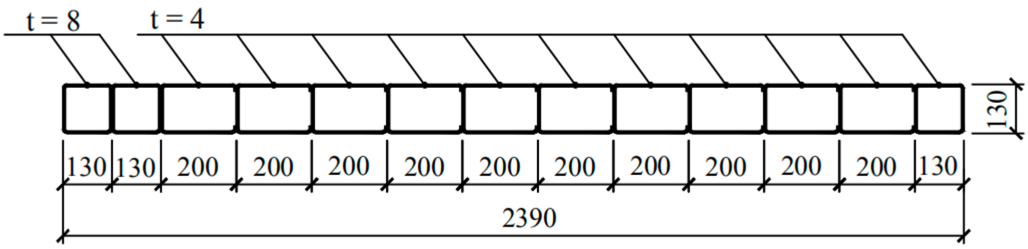

(d)

Figure 3. Geometric dimensions of specimens W1 and W2 (units in mm): (**a**) geometric dimensions of specimen W1; (**b**) geometric dimensions of specimen W2; (**c**) cross-section of the BLC-C composite wall of specimen W1; and (**d**) cross-section of the BLC-C composite wall of specimen W2.

The loading beam and foundation beam were set at the top and bottom of the specimen, respectively. The beams had sufficient strength and rigidity to ensure that no large deformation occurred during the loading process. The steel plates were welded at the ends of the BLC-C composite wall, which was connected to the loading beam and the foundation beam by high-strength bolts. A lateral support was arranged on the loading beam to prevent any out-of-plane behavior of the specimen. The foundation beam was clamped to the ground by ground anchors. In the test, a 500 t jack on the reaction wall was used to apply a unidirectional horizontal load to the loading beam in increments of 100 kN [17]. The elastic story drift angle of a BLC-C composite wall structure should not be greater than 1/400 under wind loads, in accordance with the Chinese standard T/CECS 546 "Technical standard for structures with concrete-filled multicellular steel tube walls" [18]. Hence, the experiment was loaded until the drift angle reached 1/400. According to Chen et al. [19], in the elastic stage and elastoplastic stage, the axial load ratio of a BLC-C composite wall had little effect on the strength and stiffness. Moreover, infill walls are non-structural elements and are not subjected to the axial force transmitted from the superstructure. Therefore, the test did not consider the application of an axial load to the specimen. Figure 4 illustrates the field test diagram of specimen W2.

2.2. Material Properties

A tensile test was carried out to determine the steel properties. The yield strength and the ultimate strength of the Q355 steel were 429 MPa and 642 MPa, respectively. The elastic modulus and Poisson's ratio were 192,000 MPa and 0.3, respectively. Concrete with a strength grade of C45 was used in the specimens and the tested 28 day prismatic compressive strength was 41.5 MPa. The elastic modulus was 25,500 MPa and the Poisson's ratio was 0.2. The burned shale perforated brick had a strength grade of MU10 and the actual compressive strength was 17.0 MPa. The elastic modulus was 19,500 MPa and the Poisson's ratio was 0.17. The strength grade of the cement mortar was M5 and the tested compressive strength was 4.1 MPa. The elastic modulus and Poisson's ratio were 3520 MPa and 0.24, respectively. The tensile bond strength of the anti-crack mortar and steel plate was 0.3 MPa through the test according to Chinese standard GB/T 29,756 "Test methods of physical property for dry-mix mortar" [20].

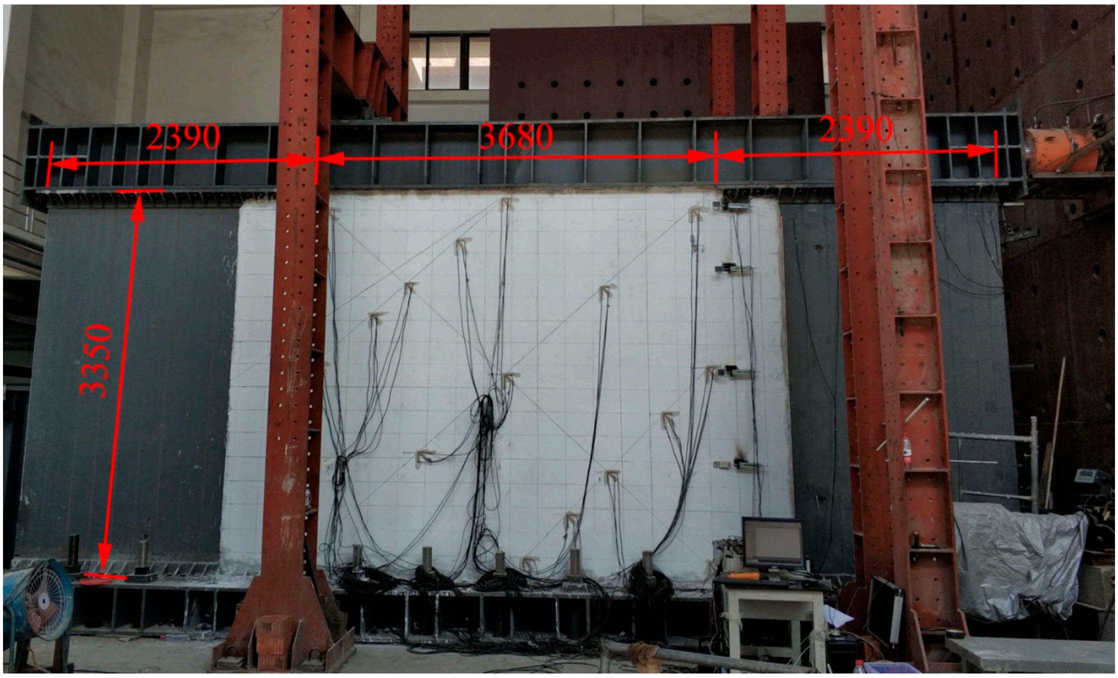

Figure 4. Field test diagram of specimen W2 (units in mm).

2.3. Experimental Phenomena

During the whole process of the test, the cracks of the interface and the infill wall were observed by a magnifying glass and a crack width card. At the start of loading, the lateral displacement of specimen W1 was small under a horizontal load and the load–displacement curve showed a linear change. When the load increased to 404 kN and the corresponding drift angle was 1/2537, the interface between the BLC-C composite wall and the infill wall initially cracked, resulting in microcracks. Oblique cracks appeared in a diagonal direction (from the bottom left to the top right) in the center of the infill wall when the load increased to 800 kN and the corresponding drift angle was 1/1015. As the load rose to 1200 kN and the corresponding drift angle was 1/557, the plaster layer between the top of the infill wall and the loaded beam exhibited slight spalling. In the center of the infill wall, penetrating diagonal cracks formed when the load grew to 1300 kN and the corresponding drift angle was 1/511. Specimen W1 was loaded until the drift angle reached 1/400.

The overall structure of specimen W2 was elastic in the early stage of loading. When the load climbed to 700 kN and the corresponding drift angle was 1/2537, interface cracks began to appear between the BLC-C composite wall and the infill wall. Diagonal cracks appeared below the center of the infill wall when the load grew to 800 kN and the corresponding drift angle was 1/1982. With an increase in the load, oblique cracks rapidly developed above and below the syncline. As the load increased to 1500 kN and the corresponding drift angle was 1/813, penetrating oblique cracks formed below the center of the infill wall. The lower right corner of the infill wall slightly separated from the foundation beam and cracks appeared when the load rose to 1600 kN and the corresponding drift angle was 1/736. Specimen W2 was also loaded until the drift angle reached 1/400. Figure 5 shows the crack distribution when the drift angle reached 1/400.

The process of specimens resisting the horizontal load could be divided into two stages. In the first stage, the elastic stage, the interface initially cracked. With an increase in the load, the number of interface cracks increased, but there was no penetrating interface crack. The BLC-C composite wall and the infill wall together constituted the lateral force-resistant components. The second stage was the elastoplastic stage. At this stage, oblique cracks appeared in the middle of the infill wall and continued to expand. The connection between the BLC-C composite walls, the steel beams, and the corner of the infill wall gradually disengaged. Furthermore, the infill wall gradually withdrew from work and the BLC-C composite wall became the main lateral force-resistant member.

(**a**)

(**b**)

Figure 5. Crack distribution diagram obtained when the drift angle reached 1/400: (**a**) specimen W1 and (**b**) specimen W2.

3. Finite Element Simulation

The finite element analysis software ANSYS was used to simulate the loading process of the tests.

3.1. Material Constitutive Relationship

All parameter values in this section refer to Section 2.2 and the related standards.

The constitutive relationship of the steel adopted the trilinear isotropic hardening model [6], including the elastic stage, strengthening section, and plastic segment.

$$\sigma = \begin{cases} E\varepsilon, & \varepsilon < \varepsilon_{\rm y}; \\ E'(\varepsilon - \varepsilon_{\rm y}) + E\varepsilon_{\rm y}, & \varepsilon_{\rm y} \le \varepsilon < \varepsilon_1; \\ E'(\varepsilon_1 - \varepsilon_{\rm y}) + E\varepsilon_{\rm y}, & \varepsilon \ge \varepsilon_1 \end{cases} \tag{1}$$

where σ and ε are the stress and strain of the steel, respectively; $\varepsilon_{\rm y}$ is the yield strain of the steel, taken as 0.0022; ε_1 is the strain at which the steel reached the ultimate tensile stress, taken as 0.0065; E is the elastic modulus of the steel, taken as 192,000 MPa; and E' is the tangent modulus of the steel, taken as 50,000 MPa.

The stress–strain relationship of the concrete conformed with the Chinese Standard GB 50010 "Code for design of concrete structures" [21].

$$\sigma{\rm c} = \begin{cases} f_{\rm c}\left[1 - \left(1 - \frac{\varepsilon_{\rm c}}{\varepsilon_0}\right)^n\right], & \varepsilon_{\rm c} \le \varepsilon_0; \\ f_{\rm c}, & \varepsilon_0 \le \varepsilon_{\rm c} \le \varepsilon_{\rm cu} \end{cases} \tag{2}$$

where $\sigma_{\rm c}$ and $\varepsilon_{\rm c}$ are the stress and strain of the concrete, respectively; $f_{\rm c}$ is the axial compressive strength of the concrete, taken as 41.5 MPa; ε_0 is the compressive strain when the concrete compressive stress reaches $f_{\rm c}$, taken as 0.002; $\varepsilon_{\rm cu}$ is the ultimate compressive strain of the concrete, taken as 0.0033; and n is the calculation coefficient, taken as 2.

The infill wall was brick masonry and the constitutive relation proposed by Turnsek and Cacovic was adopted [22].

$$\frac{\sigma_{\rm b}}{f_{\rm m}} = 6.4\left(\frac{\varepsilon_{\rm b}}{\varepsilon_0}\right) - 5.4\left(\frac{\varepsilon_{\rm b}}{\varepsilon_0}\right)^{1.17} \tag{3}$$

where $\sigma_{\rm b}$ and $\varepsilon_{\rm b}$ are the stress and strain of the brick masonry and ε_0 is the strain corresponding with $f_{\rm m}$, taken as 0.003. $f_{\rm m}$ is the average compressive strength of the brick masonry; the calculation formula referred to Chinese standard GB 50003 "Code for design of masonry structures" [23].

$$f_{\rm m} = k_1 f_1^{\alpha}(1 + 0.07 f_2)k_2 \tag{4}$$

where k_1, α, and k_2 are coefficients, taken as 0.78, 0.5, and 1, respectively; f_1 is the strength grade of the bricks, taken as 10 MPa; and f_2 is the average compressive strength of the mortar, taken as 4.1 MPa. Therefore, $f_{\rm m}$ was calculated as 3.17 MPa.

3.2. Contact Property

The contact of the finite element model included a normal contact and tangential bond slip, which mainly existed between the steel tube and the concrete as well as between the infill wall and the BLC-C composite wall. The normal contact adopted the hard contact model and the contact stiffness coefficient was set to 10 to minimize intrusion. The tangential bond slip used the Coulomb friction model and the friction coefficients between the steel tube and the concrete and between the infill wall and the BLC-C composite wall were set to 0.3 [24] and 0.45 [23], respectively.

An augmented Lagrangian method was selected for the contact algorithms. The bonded contact and the cohesive zone material models were used to simulate the connection structure of the interface between the BLC-C composite wall and the infill wall. The cohesive zone material model assumed that the stress transfer between the separate faces did not completely disappear at the debonding initiation, but rather was a gradual stiffness reduction at the interface between them [25]. The bilinear material behavior contact model CBDD was selected as the cohesive zone material model to simulate the traction separation behavior of the interface. The maximum normal contact stress was set to 0.3 MPa in accordance with the tensile bond strength of the anti-crack mortar and steel plate.

3.3. Element Type, Boundary Condition, and Solution Method

The loading and foundation beams were simulated using the shell element SHELL181. The steel tube of the BLC-C composite wall used the three-dimensional solid element SOLID45. The contact of the finite element model was simulated using the contact element CONTAC173 and the target element TARGE170. The infill wall and the concrete of the BLC-C composite wall adopted the three-dimensional solid element SOLID65, which was defined by eight nodes and could simulate cracking, crushing, plastic deformation, and creep. The smeared crack model and the failure criterion of Willam–Warnke were utilized in the simulation cracking [26]. When cracking occurred at an integration point, the cracking was modeled through an adjustment to the material properties [27]. This method is widely used and was conductive to the realization of the finite element program.

The finite element model was divided by mapping the mesh with a mesh size of 50 mm. The nodes on the contact surface of the BLC-C composite wall and the steel beam were coupled through the translational degrees of freedom in the x, y, and z directions to simulate the bolt connection. All the degrees of freedom of the nodes on the bottom of the foundation beam were restrained and the displacement load acted on the end of the loading beam. A full Newton–Raphson analysis with unsymmetric matrices of elements was used to solve the non-linear equations in the finite element analysis. For the convergence criteria, the tolerance was 5% for the force and displacement. Figure 6 shows the finite element model of specimen W2.

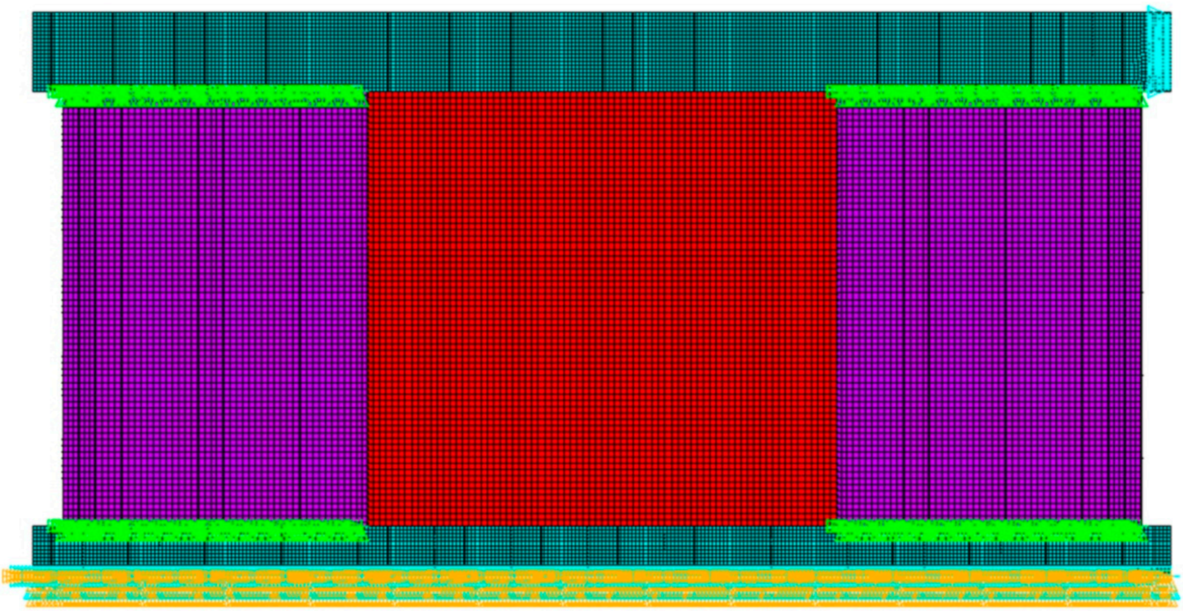

Figure 6. Finite element model of specimen W2.

3.4. Simulation Results

According to the finite element modeling method described above, finite element models were established to simulate the two specimens. The load–displacement curves obtained from the experiment and finite element analysis are illustrated in Figure 7. The load errors when the displacement was 8.38 mm (i.e., at a drift angle of 1/400) of specimens W1 and W2 were 5.5% and 5.0%, respectively. The load–displacement curves of the simulation and experiment were similar and the finite element simulation was consistent with the experiment.

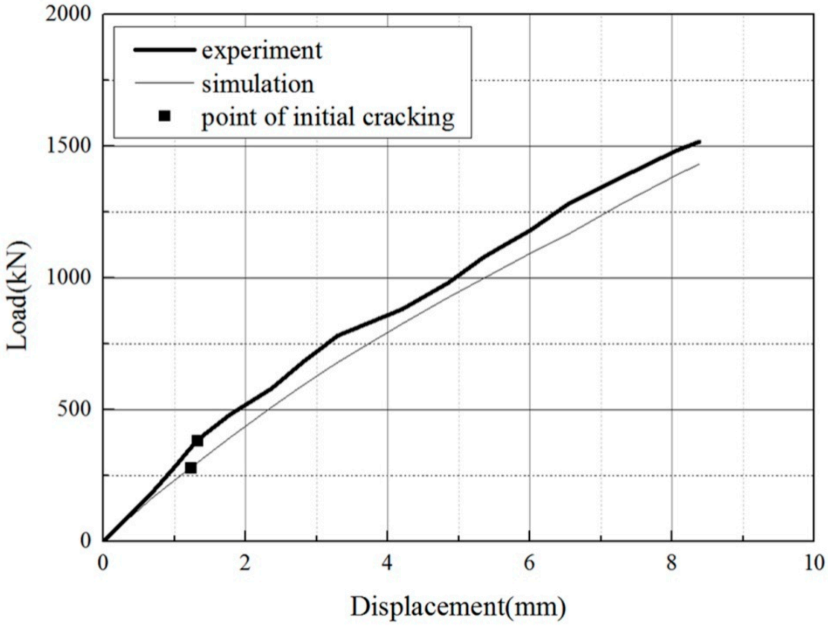

(a)

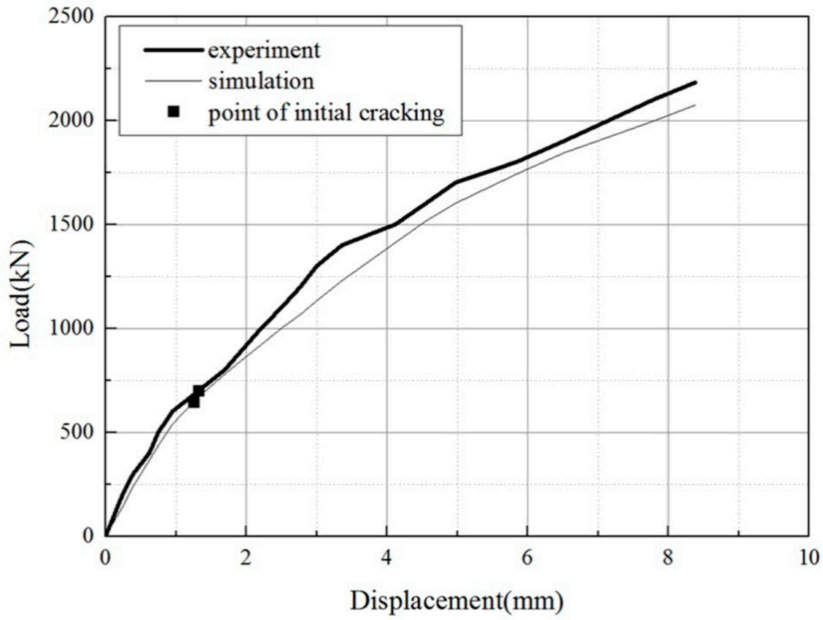

(b)

Figure 7. Load–displacement curves obtained from the experiment and finite element calculations: (**a**) specimen W1 and (**b**) specimen W2.

In the test, when the horizontal displacements of specimens W1 and W2 were both 1.32 mm (i.e., the drift angle was 1/2537), initial cracks occurred at the interface between the

BLC-C composite wall and the infill wall. The crack distribution diagram of W2 when the interface initially cracked in the experiment is presented in Figure 8. In the finite element analysis, when the infill wall began to crack at the interface position, it was considered that the interface initially cracked. Figure 9 shows the crack distribution diagram of W2 when the interface initially cracked in the finite element simulation. In the finite element simulation, the horizontal displacements of specimens W1 and W2 at the initial interface cracking were 1.23 and 1.25 mm, respectively. In comparison with the experiment, the errors were 6.8% and 5.3%, respectively, demonstrating good consistency.

Figure 8. Diagram of specimen W2 in the experiment when the interface initially cracked and the horizontal displacement was 1.32 mm.

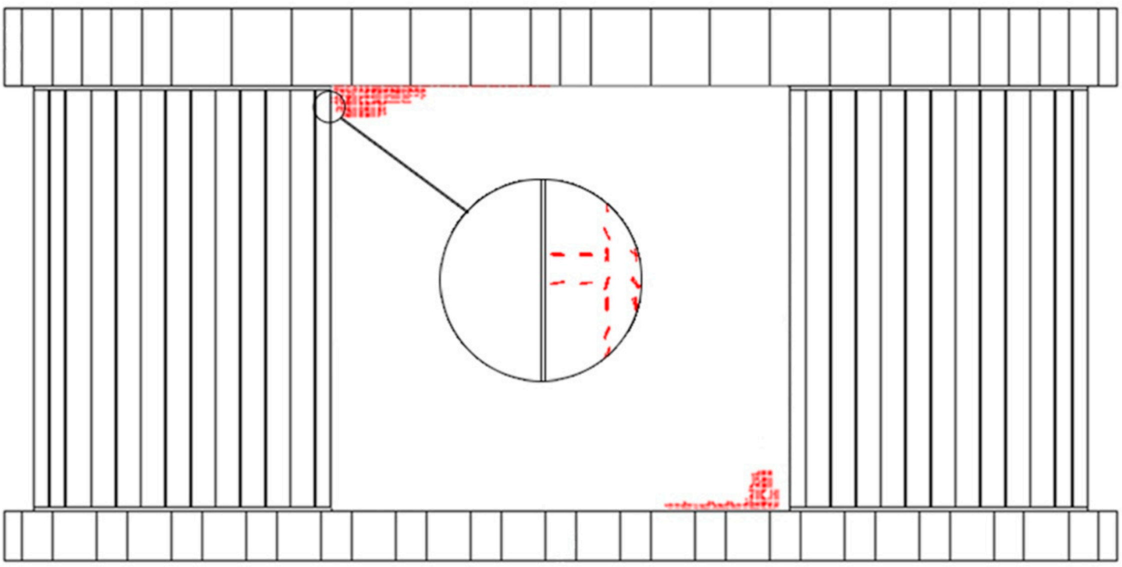

Figure 9. Diagram of specimen W2 in the simulation when the interface initially cracked and the horizontal displacement was 1.25 mm.

Diagonal cracks appeared in the infill walls of W1 and W2 in the experiment; the maximum principal stress cloud diagram of the finite element simulation at this time is depicted in Figure 10. The maximum principal stress was larger in the center of the infill wall in the direction of the reverse diagonal (from the top left to the bottom right), resulting in diagonal cracks. This finding was consistent with the test phenomena. Figure 11 is the crack distribution diagram of when the displacement was 8.38 mm (i.e., at a drift angle of 1/400) in the simulation, which was relatively similar to that in the experiment (Figure 5). To sum up, the finite element model could precisely simulate the mechanical characteristics of the infill wall constrained by the BLC-C composite walls on both sides.

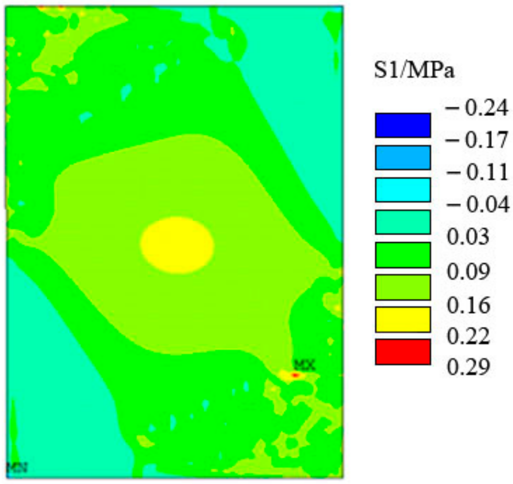

(**a**)

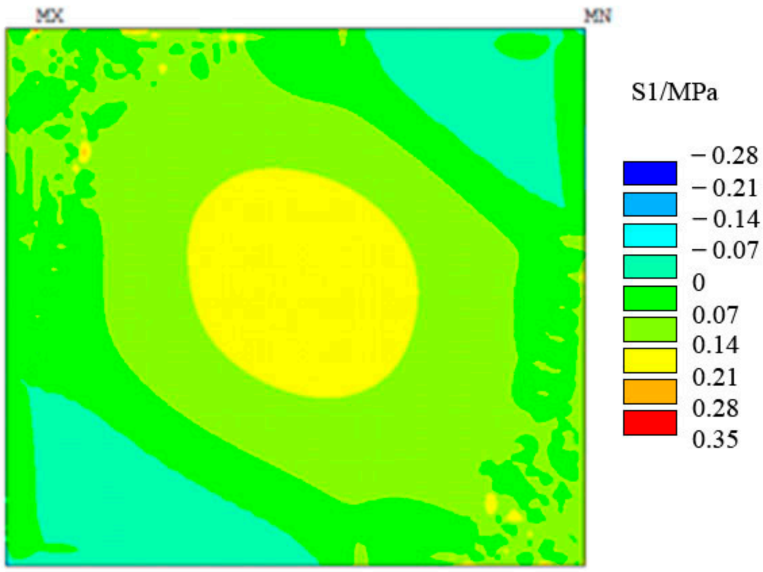

(**b**)

Figure 10. Maximum principal stress cloud diagram: (**a**) specimen W1 and (**b**) specimen W2.

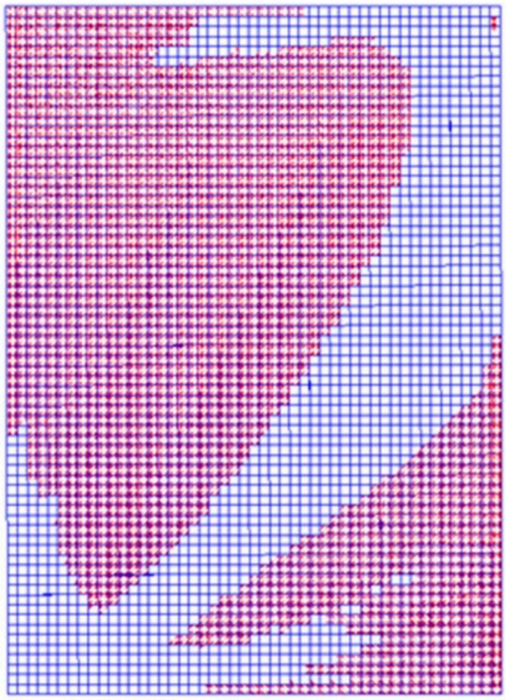

(**a**)

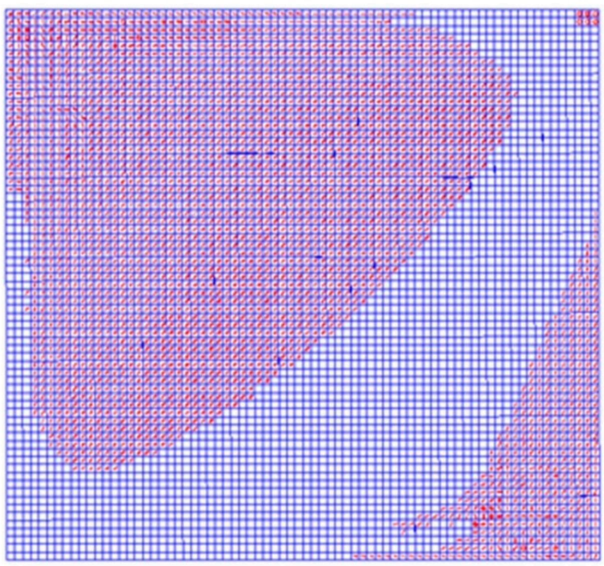

(**b**)

Figure 11. Crack distribution diagram obtained by finite element simulation when the drift angle reached 1/400: (**a**) specimen W1 and (**b**) specimen W2.

4. Analysis of the Initial Interface Cracking

A parametric analysis was conducted to determine the effects of various factors on the horizontal displacement when the interface between the BLC-C composite wall and the infill wall initially cracked. The factors included the widths of the BLC-C composite wall, infill wall, and opening of the infill wall as well as the strength grade of the bricks and maximum normal contact stress. The finite element model of specimen W2 was used as the standard model and the finite element analysis was conducted by varying the factors.

4.1. Width of the BLC-C Composite Wall

The width of the BLC-C composite wall was altered to determine its effect on the horizontal displacement at the initial interface cracking; the other factors were maintained as constants. As depicted in Figure 12, when the width of the BLC-C composite wall decreased from 2390 mm to 1930, 1730, 1530, 1130, and 730 mm, the horizontal displacement at the initial interface cracking grew from 1.25 mm to 1.35, 1.43, 1.58, 1.74, and 1.84 mm, respectively. With an increase in the width of the BLC-C composite wall, the horizontal displacement at the initial cracking of the interface dropped and the appearance of interface cracks occurred earlier.

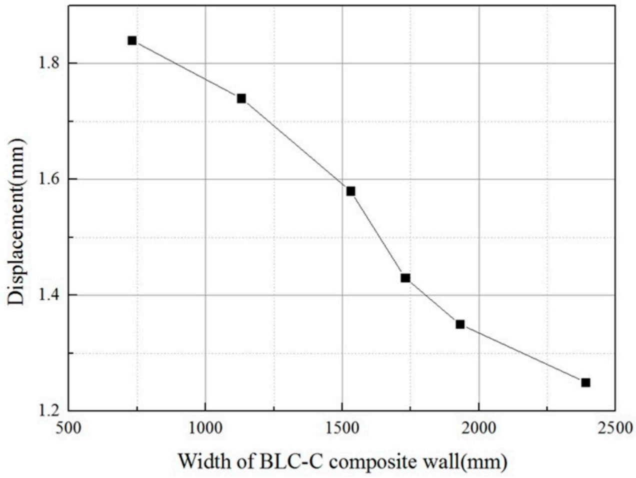

Figure 12. Variation curve of the horizontal displacement at the initial cracking of the interface with the width of BLC-C composite wall.

4.2. Width of the Infill Wall

Whilst maintaining the other parameters as constants, the width of the infill wall was varied to study its effect on the horizontal displacement when the interface initially cracked. Figure 13 shows that the horizontal displacement at the initial interface cracking changed from 1.25 mm to 2.71, 0.78, 0.32, and 0.26 mm when the width of the infill wall altered from 3680 mm to 4000, 3000, 2500, and 2000 mm, respectively. This finding suggested that as the width of the infill wall widened, the horizontal displacement at the initial cracking of the interface rose and the appearance of interface cracks occurred later.

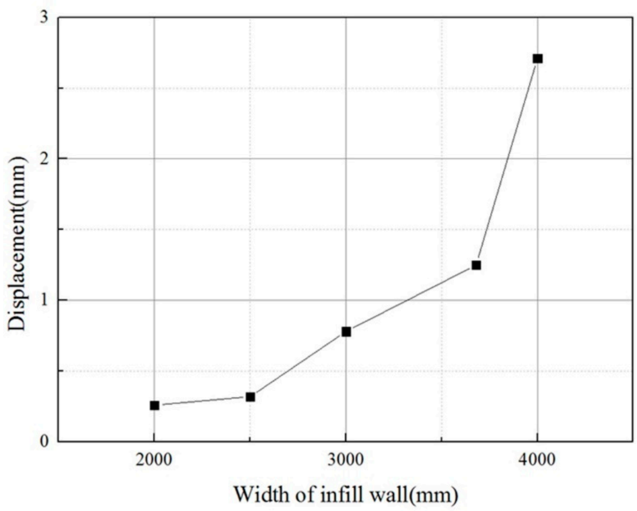

Figure 13. Variation curve of the horizontal displacement at the initial cracking of the interface with the width of infill wall.

4.3. Width of the Opening

The location of the opening is shown in Figure 14. The width of the opening was changed whilst maintaining the other parameters as constants to determine its influence on the horizontal displacement at the initial cracking of the interface. The horizontal center of the opening was always the same as the horizontal center of the infill wall. Figure 15 shows that when the infill wall was altered from no opening to openings of 1200 × 1900, 2050 × 1900, 2450 × 1900, and 2850 × 1900 mm, the horizontal displacement at the initial interface cracking varied from 1.25 mm to 1.43, 1.58, 1.88, and 2.53 mm, respectively. This finding implied that an increase in the width of the opening led to an increase in the horizontal displacement at the initial cracking of the interface and the delayed appearance of interface cracks.

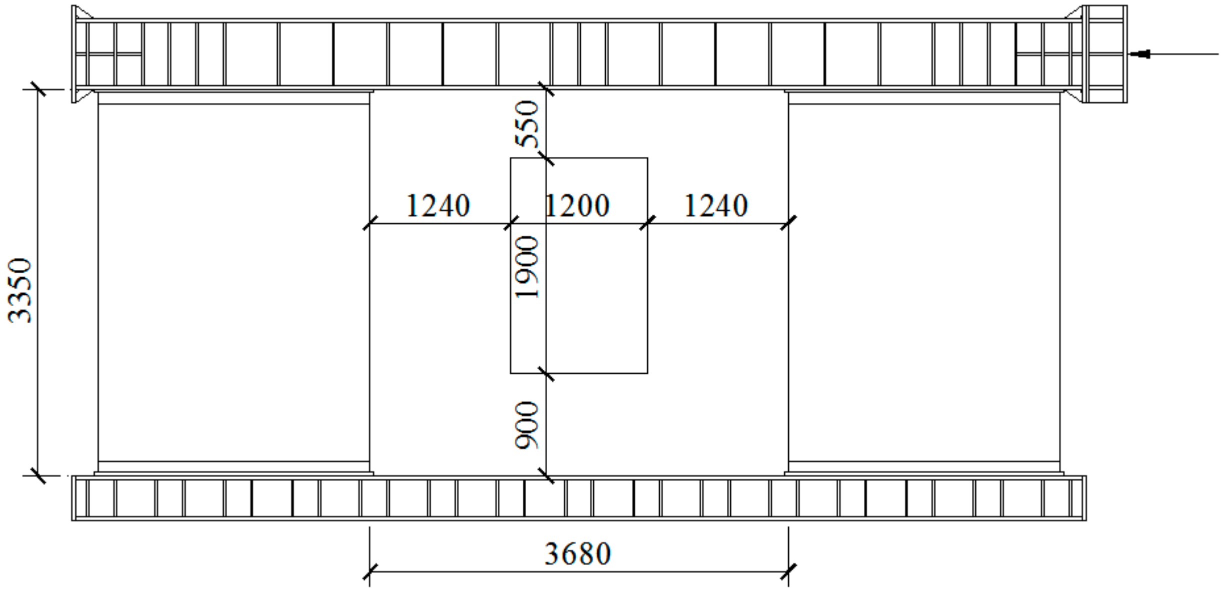

Figure 14. Location of the opening (units in mm).

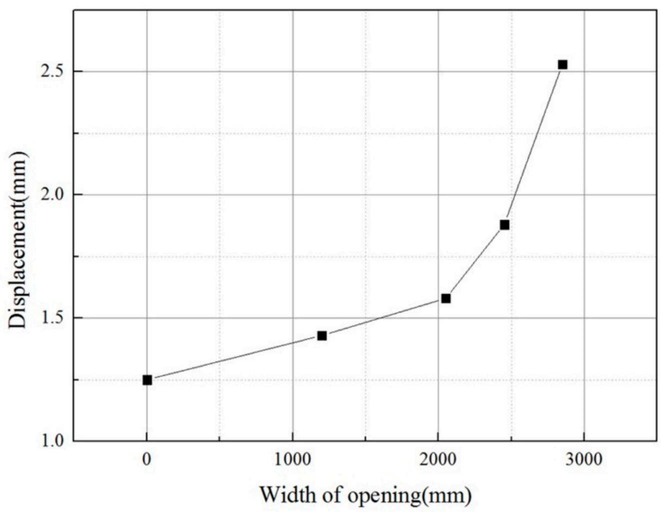

Figure 15. Variation curve of the horizontal displacement at the initial cracking of the interface with the width of opening.

4.4. Strength Grade of the Bricks

The strength grade of the bricks was altered to examine its effect on the horizontal displacement when the interface initially cracked. As shown in Figure 16, when the strength grade of the bricks varied from MU10 to MU15, MU20, MU25, and MU30, the horizontal displacement at the initial interface cracking changed from 1.25 mm to 1.00, 0.79, 0.67, and 0.65 mm, respectively. Due to the rise in the strength grade of the bricks, the horizontal displacement at the initial cracking of the interface decreased and the interface crack appeared earlier.

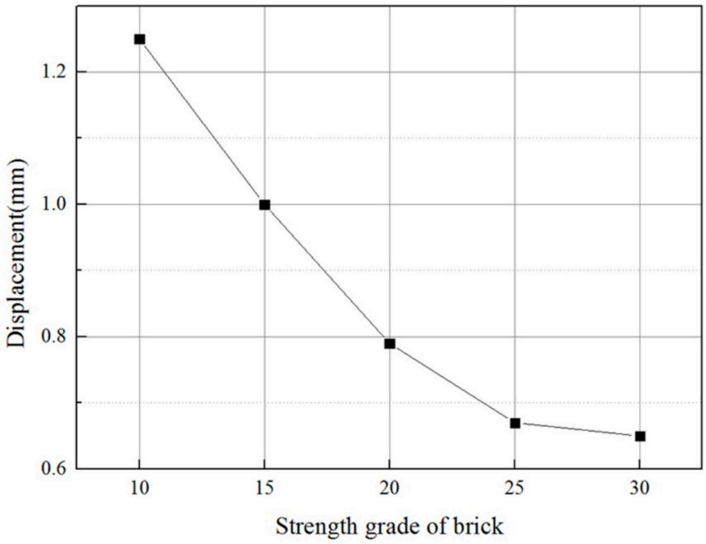

Figure 16. Variation curve of the horizontal displacement at the initial cracking of the interface with the strength grade of bricks.

4.5. Maximum Normal Contact Stress

The maximum normal contact stress between the BLC-C composite wall and the infill wall was changed to investigate its influence on the horizontal displacement when the interface initially cracked. Figure 17 shows that the horizontal displacement at the initial interface cracking varied from 1.25 mm to 0.52, 0.89, 1.53, and 1.76 mm when the maximum normal contact stress changed from 0.3 MPa to 0.1, 0.2, 0.4, and 0.5 MPa, respectively. The horizontal displacement at the initial cracking of the interface grew and the interface crack appeared later due to the rise in the maximum normal contact stress.

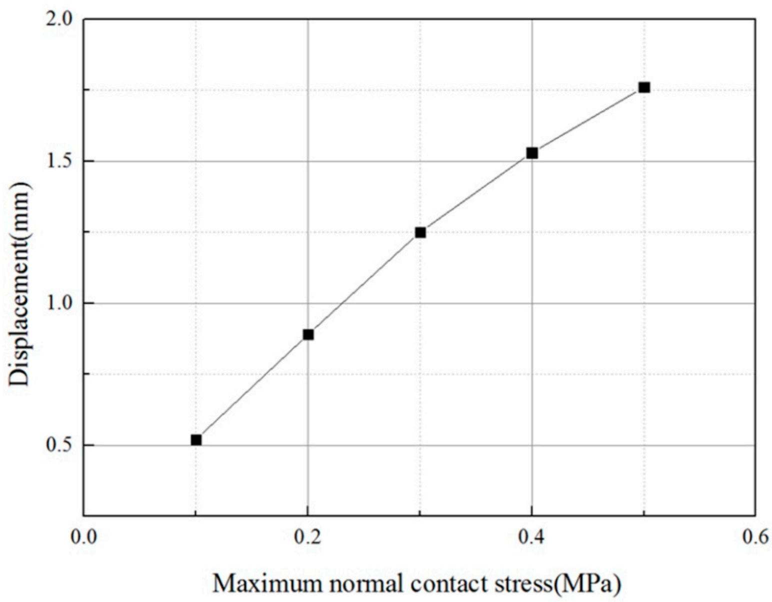

Figure 17. Variation curve of the horizontal displacement at the initial cracking of the interface with the maximum normal contact stress.

4.6. Discussion

In previous research on masonry-infilled reinforced concrete frames, the stiffness of the bare frame was less than the stiffness of the infill wall. The frame-to-infill stiffness ratio played a key role in the infill–frame contact length. An increase in the stiffness of the frame increased the contact length [28,29]. On the contrary, in our experiment the stiffness of the BLC-C composite wall was greater than the infill wall due to the high steel content. When the stiffness of the BLC-C composite wall fell or the stiffness of the infill wall rose, the contact length grew. Therefore, a decrease in the width of the BLC-C composite wall or an increase in the width of the infill wall improved the collaborative deformation ability and delayed the appearance of interface cracks.

On the other hand, previous literature [12,30,31] has shown that the greater the opening size, the greater the infill–frame contact length. Similarly, in our finite element analysis, a large opening increased the contact length, caused the curvature of the infill wall to follow the curvature of the BLC-C composite wall, and delayed the appearance of interface cracks.

According to the finite element calculation results, the horizontal displacement at the initial cracking of the interface increased with an increase in the maximum normal contact stress between the BLC-C composite wall and the infill wall. Therefore, strengthening the tensile bond strength of the mortar and steel plate could help delay the appearance of interface cracks. For example, in the connection structure of an interface, an interface mortar could be developed and employed on the surface of the steel to enhance the tensile bond strength. As for the strength grade of the bricks, there is a lack of relevant research and it should be further investigated in future studies.

5. Conclusions

The finite element software ANSYS was used to simulate a unidirectional horizontal loading test of an infill wall constrained by BLC-C composite walls on both sides. The finite element model was validated through experimentation and the main conclusions are as follows.

(1) Within the elastic story drift limit, the experiment process was divided into an elastic stage and an elastoplastic stage. In the elastic stage, the BLC-C composite wall and the infill wall acted as the lateral force-resistant members. In the elastoplastic stage, the BLC-C composite wall became the main lateral force-resistant member.
(2) The load–displacement curves and crack distribution images obtained from the finite element simulation were similar to the test results. Therefore, the finite element model proposed in this study could be used to accurately simulate an actual deformation process.
(3) A decrease in the width of the BLC-C composite wall or an increase in the width of the infill wall delayed the appearance of interface cracks.
(4) A large opening delayed the appearance of interface cracks.
(5) An enhancement in the strength grade of the bricks led to the earlier appearance of interface cracks.
(6) When the maximum normal contact stress rose, the interface cracks occurred later. Therefore, in order to delay the appearance of interface cracks, it is recommended that the tensile bond strength of the mortar and the steel plate in the connection structure of the interface are reinforced.

The out-of-plane behavior of the specimens was also of importance. However, a lateral support was used in this test to prevent the out-of-plane behavior of the specimen. Hence, this paper did not address the out-of-plane behavior of the specimen. Our research group aims to research this further in the future.

Author Contributions: Conceptualization, P.C. and L.Z.; methodology, L.Z.; software, P.C.; validation, X.Q.; formal analysis, P.C.; resources, S.R.; data curation, G.L.; writing—original draft preparation, P.C.; writing—review and editing, P.C.; supervision, K.Q.; project administration, X.Q. All authors have read and agreed to the published version of the manuscript.

Funding: This research received no external funding.

Conflicts of Interest: The authors declare no conflict of interest.

References

1. Zhang, X.; Qin, Y.; Chen, Z. Experimental seismic behavior of innovative composite shear walls. *J. Constr. Steel Res.* **2016**, *116*, 218–232. [CrossRef]
2. Li, Y.; Cao, S.; Chen, Z.; Li, W.; Hu, L. Experiment on seismic performance of bundled lipped channel-concrete composite wall and beam-flange-strengthened connections. *J. Tianjin Univ. (Sci. Technol.)* **2016**, *49*, 41–47. Available online: https://kns.cnki.net/kcms/detail/detail.aspx?FileName=TJDX2016S1007&DbName=CJFQ2016 (accessed on 15 July 2016). (In Chinese)
3. Sun, H.; Wan, Q.; Yang, Q.; Li, H. Finite element analysis on axial compression behavior of steel tube confined concrete shear wall. *J. Guilin Univ. Technol.* **2019**, *39*, 628–634. Available online: http://manu28.magtech.com.cn/Jweb_gllg/CN/Y2019/V39/I3/628 (accessed on 6 September 2019). (In Chinese)
4. Zhang, X.; Qin, Y.; Chen, Z.; Jie, L. Experimental behavior of innovative T-shaped composite shear walls under in-plane cyclic loading. *J. Constr. Steel Res.* **2016**, *120*, 143–159. [CrossRef]
5. Li, J.; Chen, Z.; Zhang, X.; Yang, Q.; Li, W.; Hu, L. Experimental study on seismic performance of connections between bundled lipped channel-concrete (BLC-C) composite wall and steel beam. *J. Vib. Shock* **2016**, *35*, 159–165. Available online: https://www.cnki.net/kcms/doi/10.13465/j.cnki.jvs.2016.21.025.html (accessed on 15 November 2016). (In Chinese)
6. Chen, Z.H.; Jiang, Y.T.; Zhang, X.M.; Yang, Q.Y.; Li, W.B. Parametric analysis and calculation method for bending and shear capacities of innovative composite shear walls. *Adv. Struct. Eng.* **2017**, *20*, 1046–1058. [CrossRef]
7. Guo, L.; Wang, Y.; Zhang, S. Experimental study of rectangular multi-partition steel-concrete composite shear walls. *Thin-Walled Struct.* **2018**, *130*, 577–592. [CrossRef]
8. Sun, H.; Xu, Q.; Yan, P.; Yin, J.; Lou, P. A study on axial compression performance of concrete-filled steel-tubular shear wall with a multi-cavity T-shaped cross-section. *Energies* **2020**, *13*, 4831. [CrossRef]
9. Mondal, G.; Jain, S.K. Lateral Stiffness of Masonry Infilled Reinforced Concrete (RC) Frames with Central Opening. *Earthq. Spectra* **2008**, *24*, 701–723. [CrossRef]
10. Hashemi, A.; Mosalam, K.M. Shake-table experiment on reinforced concrete structure containing masonry infill wall. *Earthq. Eng. Struct. Dyn.* **2006**, *35*, 1827–1852. [CrossRef]
11. Chrysostomou, C.Z.; Asteris, P.G. On the in-plane properties and capacities of infilled frames. *Eng. Struct.* **2012**, *41*, 385–402. [CrossRef]
12. Asteris, P.G.; Cavaleri, L.; Trapani, F.; Di Sarhosis, V. A macro-modelling approach for the analysis of infilled frame structures considering the effects of openings and vertical loads. *Struct. Infrastruct. Eng.* **2015**, *12*, 551–566. [CrossRef]
13. Asteris, P.G.; Cavaleri, L.; Di Trapani, F.; Tsaris, A.K. Numerical modelling of out-of-plane response of infilled frames: State of the art and future challenges for the equivalent strut macromodels. *Eng. Struct.* **2017**, *132*, 110–122. [CrossRef]
14. Buonopane, S.G.; White, R.N. Pseudodynamic Testing of Masonry Infilled Reinforced Concrete Frame. *J. Struct. Eng.* **1999**, *125*, 578–589. [CrossRef]
15. Koutromanos, I.; Stavridis, A.; Shing, P.B.; Willam, K. Numerical modeling of masonry-infilled RC frames subjected to seismic loads. *Comput. Struct.* **2011**, *89*, 1026–1037. [CrossRef]
16. *GB 50011*; Code for Seismic Design of Buildings. Ministry of Housing and Urban-Rural Construction of the People's Republic of China: Beijing, China, 2010.
17. Chen, Y.; Li, Y.; Xie, C.; Qian, K.; Zhang, Y.; Cheng, P.; Ye, X. Pushover test study of masonry structure restrained by steel-tube-bundle shear walls. *J. Zhejiang Univ. (Eng. Sci.)* **2020**, *54*, 499–511. (In Chinese) [CrossRef]
18. *T/CECS 546*; Technical Standard for Structures with Concrete-Filled Multicellular Steel Tube Walls. China Association for Engineering Construction Standardization: Beijing, China, 2018.
19. Chen, Z.; Jiang, Y.; Zhang, X.; Yang, Q.; Li, W. Research on resilience model of steel tube bundle composite shear wall. *Earthq. Eng. Eng. Dyn.* **2017**, *37*, 115–122. (In Chinese)
20. *GB/T 29756*; Test Methods of Physical Property for Dry-Mix Mortar. State Administration for Market Regulation of the People's Republic of China: Beijing, China, 2013.
21. *GB 50010*; Code for Design of Concrete Structures. Ministry of Housing and Urban-Rural Construction of the People's Republic of China: Beijing, China, 2010.
22. Turnšek, V.; Čačovič, F. Some experimental results on the strength of brick masonry walls. In Proceedings of the 2nd International Brick Masonry Conference, Stoke-on-Trent, UK, 12–15 April 1970; pp. 149–156. Available online: http://www.hms.civil.uminho.pt/ibmac/1970/149.pdf (accessed on 1 January 1971).
23. *GB 50003*; Code for Design of Masonry Structures. Ministry of Housing and Urban-Rural Construction of the People's Republic of China: Beijing, China, 2010.
24. Li, G.; Yu, Y.; Gu, Q. Finite element analysis for concrete infilled steel frame. *Sichuan Build. Sci.* **2007**, *33*, 4. Available online: https://kns.cnki.net/kcms/detail/detail.aspx?FileName=ACZJ200705006&DbName=CJFQ2007 (accessed on 25 October 2007). (In Chinese)

25. Shabana, I.S.; Sharaky, I.A.; Khalil, A.; Hadad, H.S.; Arafa, E.M. Flexural response analysis of passive and active near-surface-mounted joints: Experimental and finite element analysis. *Mater. Struct.* **2018**, *51*, 107. [CrossRef]
26. Dahmani, L.; Khennane, A.; Kaci, S. Crack identification in reinforced concrete beams using ANSYS software. *Strength. Mater.* **2010**, *42*, 232–240. [CrossRef]
27. Yan, F.; Lin, Z. Bond behavior of GFRP bar-concrete interface: Damage evolution assessment and FE simulation implementations. *Compos. Struct.* **2016**, *155*, 63–76. [CrossRef]
28. Alwashali, H.; Torihata, Y.; Jin, K.; Maeda, M. Experimental observations on the in-plane behaviour of masonry wall infilled RC frames; focusing on deformation limits and backbone curve. *Bull. Earthq. Eng.* **2018**, *16*, 1373–1397. [CrossRef]
29. Trapani, F.D.; Macaluso, G.; Cavaleri, L.; Papia, M. Masonry infills and RC frames interaction: Literature overview and state of the art of macromodeling approach. *Eur. J. Environ. Civ. Eng.* **2015**, *19*, 1059–1095. [CrossRef]
30. Asteris, P.G. Lateral stiffness of brick masonry infilled plane frames. *J. Struct. Eng.* **2003**, *129*, 1071–1079. [CrossRef]
31. Smith, B.S. Model test results of vertical and horizontal loading of infilled frames. *J. Proc.* **1968**, *65*, 618–625. Available online: https://www.concrete.org/publications/internationalconcreteabstractsportal/m/details/id/7499 (accessed on 1 January 1971).